This is a repository copy of *Long-distance continuous-variable quantum key distribution over 202.81 km fiber*.

Long-distance continuous-variable quantum key distribution over 202.81 km fiber

Yichen Zhang[1], Ziyang Chen[2], Stefano Pirandola[3], Xiangyu Wang[1], Chao Zhou[1], Binjie Chu[1], Yijia Zhao[1], Bingjie Xu[4], Song Yu[1],[*] and Hong Guo[2][†]

[1]*State Key Laboratory of Information Photonics and Optical Communications,*
Beijing University of Posts and Telecommunications, Beijing 100876, China
[2]*State Key Laboratory of Advanced Optical Communication Systems and Networks, Department of Electronics,*
and Center for Quantum Information Technology, Peking University, Beijing 100871, China
[3]*Computer Science and York Centre for Quantum Technologies,*
University of York, York YO10 5GH, United Kingdom and
[4]*Science and Technology on Security Communication Laboratory,*
Institute of Southwestern Communication, Chengdu 610041, China
(Dated: June 6, 2020)

Quantum key distribution provides secure keys resistant to code-breaking quantum computers. The continuous-variable version of quantum key distribution offers the advantages of higher secret key rates in metropolitan areas, as well as the use of standard telecom components that can operate at room temperature. However, the transmission distance of these systems (compared with discrete-variable systems) are currently limited and considered unsuitable for long-distance distribution. Herein, we report the experimental results of long distance continuous-variable quantum key distribution over 202.81 km of ultralow-loss optical fiber by suitably controlling the excess noise and employing highly-efficient reconciliation procedures. This record-breaking implementation of the continuous-variable quantum key distribution doubles the previous distance record and shows the road for long-distance and large-scale secure quantum key distribution using room-temperature standard telecom components.

Introduction. − The BB84 protocol [1] started the era of quantum key distribution (QKD) [1–4], providing a way to securely generate secret keys between two remote users by exploiting the laws of quantum mechanics. Combining this method with one-time pad provides ultimate physical-layer protection to the transmission of confidential messages. In general, for cost-effective implementations, QKD protocols are formulated in a prepare-and-measure fashion, where classical information is encoded in non-orthogonal quantum states: these are randomly prepared by Alice (the sender) and then transmitted to Bob (the receiver) through an insecure quantum channel. At the output of the channel, the states will be measured by Bob, so as to retrieve the encoded classical information. Depending on the setting, this measurement may consist of single-photon detections or coherent measurements, such as homodyne or heterodyne detections. The latter are certainly more attractive for commercial deployment, due to their room-temperature operation and compatibility with the current telecommunication infrastructure [5–8]. Protocols that exploit such coherent measurements and encode classical information by modulating states of an optical mode are today very popular and known as continuous-variable QKD (CV-QKD) protocols [3, 9–11].

The most known CV-QKD protocol is the seminal GG02 protocol: this is based on the Gaussian modulation of the amplitudes of coherent states and homodyne detection of the channel output [12, 13]. This protocol later evolved into various other Gaussian protocols [14–16] and it has been the subject of increasingly-refined security proofs [17–20]. Many experimental demonstrations of GG02 [21, 22] and oth-

er CV-QKD protocols have been achieved so far (e.g., see [3, Sec. VIII] for an overview). The longest distance achieved in CV-QKD is currently 100 km in fiber, with a secure key rate of the order of 50 bps [22]. Compared to the performance of discrete-variable (DV) QKD protocols, this is a limited transmission distance with a relatively low key rate.

Here, we report the longest-distance experimental demonstration of CV-QKD, paving the way for closing the gap with the current performance of DV-QKD protocols. In fact, our experiment realizes CV-QKD over the record-breaking distance of about 200 km of fiber channel, doubling the previous record [22]. More precisely, we achieve the secret key rate of 6.214 bps at a distance of 202.81 km of ultralow-loss optical fiber. We obtain this result thanks to a fully automatic control system and high-precision phase compensation, so that the excess noise can be kept down to reasonably low values. In our experiment, we also use different reconciliation strategies at the various experimental distances considered, with an efficiency of 98% for the longest point at 202.81 km.

Experimental Setup. − Our experimental setup is shown in Fig. 1. At Alice's side, continuous-wave coherent light is generated by a 1550 nm commercial laser diode with a narrow linewidth of 100 Hz (NKT BasiK E15). Two cascaded amplitude modulators (AM$_1$ and AM$_2$, iXblue, MXER-LN-10-PD), each with high optical extinction of 45 dB, generate light pulses at a repetition rate of 5 MHz. A very unbalanced 1/99 beamsplitter (General Photonics) divides the pulses into strong local oscillator (LO) pulses and weak signal pulses. The latter are modulated by an amplitude modulator (AM$_3$, Optilab, IM-1550-12-PM) with Rayleigh distribution and a phase modulator (PM$_1$, EOSPACE, PM-OSES-10-PFA-PFA) with uniform distribution to get the zero-centered Gaussian distributions. For security reasons, the signal pulses are then attenuated to a several-photon level by using another ampli-
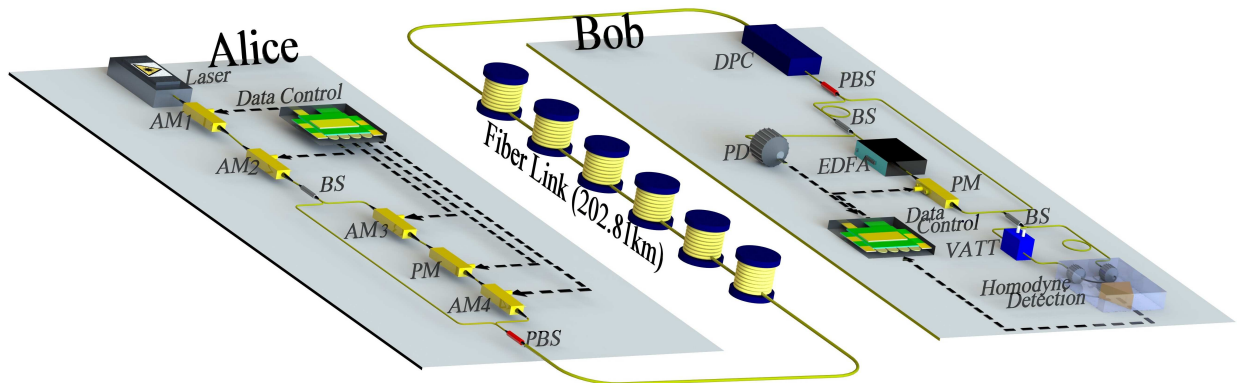
FIG. 1. Optical layout of our long-distance CV-QKD system. Alice sends an ensemble of 38 ns weak Gaussian-modulated coherent states to Bob multiplexed with a strong local oscillator (LO) in time and polarization by using a delay line and a polarization beam-combiner, respectively. Then the two optical paths are demultiplexed at Bob's side by a polarizing beamsplitter placed after an active dynamic polarization controller. We perform phase modulation on the LO path to select the signal quadrature randomly. Finally, the quantum signal interferes with the LO on a shot-noise-limited balanced pulsed homodyne detector. Laser: continuous-wave laser; AM: amplitude modulator; PM: phase modulator; BS: beamsplitter; VATT: variable attenuator; PBS: polarization beamsplitter; DPC: dynamic polarization controller; EDFA: Erbium doped fiber amplifier; PD: photodetector.

tude modulator (AM$_4$, iXblue, MXER-LN-10-PD). Finally, the signal pulses are recombined with the LO pulses in a polarizing beamsplitter and sent to Bob, each with a duration period of 38 ns.

At the output of the fiber link, signal and LO pulses are demultiplexed by another polarizing beamsplitter which is placed after an active dynamic polarization controller whose aim is to optimize the outputs. On the LO path, a customized Erbium doped fiber amplifier consisting of ultra narrow-band optical transmission filter (about 0.5 GHz @ 1550.12 nm) is employed for amplifying the co-propagated and decreased-power LO to a magnitude that is large enough to amplify the weak quantum signal. A phase modulator (PM$_2$, EOSPACE, PM-5K4-10-PFA-PFA-UV) on the LO path selects the signal quadrature components randomly. The signal path is randomly switched off to do the real time shot-noise unit calibration [23]. The signal pulses interfere with the LO pulses on a self-developed shot-noise-limited balanced pulsed homodyne detector whose output is proportional to the signal and LO intensity.

For the fiber link, we have used an ultralow-loss ITU-T G.652 standard compliant fiber (Corning® SMF-28® ultralow-loss fiber) [24]. The average fiber attenuation (without splices) is 0.16 dB/km at 1550 nm. Our 202.81 km link has a total loss 32.45 dB. This is equivalent to 162.25 km of standard fiber with attenuation of 0.20 dB/km. Besides the longest distance of 202.81 km fiber link, the experiments with 27.27 km, 49.30 km, 69.53 km, 99.31 km, 140.52 km fiber link have also been done to show the performance of the CV-QKD system at different distances. Note, the scheme with the transmitted LO may open loopholes for the eavesdropper to intercept the secret keys by manipulating the intensity of LO pulses [25, 26]. To prevent such side-channel attacks, in the experiment, the photodiode for the synchronization is also used for the LO monitoring and we will randomly switch off the signal pulses to do the real time shot-noise unit cal-

ibration [23]. Thus, the system is immune to most current side-channel attacks against LO. A better way to avoid these attacks is to generate the LO "Locally" at Bob with a second laser [27, 28].

To overcome the channel perturbations due to the long-distance fiber, we employ several automatic feedback systems to calibrate polarization and phase and implement clock and data synchronization. Clock synchronization and data synchronization is implemented by splitting a part of the LO pulses, after their demultiplexing at Bob's side, and detecting them by using a photodiode. The detection results are feed into a clock chip to generate the high-frequency clock signals as the
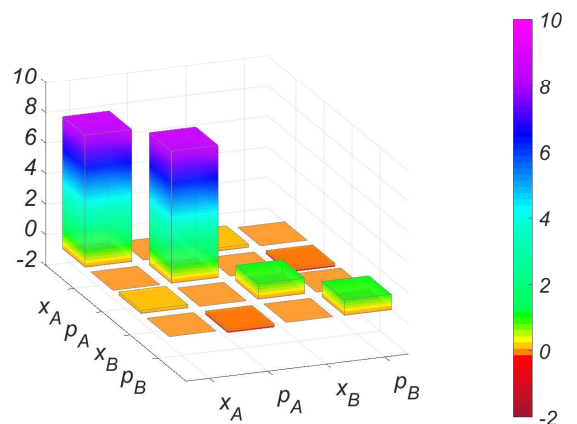

FIG. 2. Covariance matrix. We depict the covariance matrix of Alice's and Bob's variables after 202.81 km of fiber link transmission, which is based on the calibrated parameters in TABLE I using a standard expression. This follows the ordering $\{x_A, p_A, x_B, p_B\}$ and its components are expressed in shot-noise units.

TABLE I. Overview of experimental parameters and performances for different fiber lengths. SNR: signal-to-noise ratio; β: reconciliation efficiency; α: system overhead; *FER*: frame error rate of the reconciliation; V_A: modulation variance; ξ: excess noise at the channel input; ξ': worst-case excess noise estimator at the channel input; ν_{el}: electronic noise; P_{LO} : power of LO inside homodyne detector; η: efficiency of the homodyne detector; K_{finite}: final secret key rate in the finite-size regime. SNU: shot-noise unit.

Attenuation (dB)	4.36	8.29	11.68	15.89	23.46	32.45
Length (km)	27.27	49.30	69.53	99.31	140.52	202.81
SNR	2.8035	1.0715	0.4619	0.1806	0.0308	0.0023
β (%)	95.00	95.00	96.00	96.00	96.00	98.00
α (%)	10	10	10	10	10	10
FER (%)	50	50	10	10	10	90
V_A (SNU)	14.37	14.14	14.12	14.53	14.23	7.65
ξ (SNU)	0.0015	0.0033	0.0049	0.0063	0.0086	0.0081
ξ' (SNU)	0.0016	0.0037	0.0058	0.0085	0.0219	0.0383
ν_{el} (SNU)	0.1216	0.1881	0.2411	0.1893	0.2717	0.1523
P_{LO} (μW)	24.50	14.96	11.09	14.85	9.57	19.07
η (%)	61.34	61.34	61.34	61.34	61.34	61.34
K_{finite} (bps)	2.78×10^5	0.62×10^5	4.28×10^4	1.18×10^4	318.85	6.214

time baseline for the overall system. Combined with the inserted specific training sequences before the data frame for the modulation on AM$_1$, data synchronization is thus realized using this detection output of the photodiode by distinguishing the training sequences. The polarization calibration module aims to compensate the polarization drift during the transmission through the quantum channel, including the aforementioned polarization beamsplitter and photodiode, and another key component, i.e., a dynamic polarization controller. The output of the photodiode is a feedback signal which is used for adjusting the dynamic polarization controller so as to let the LO power larger than that of the signal up to 30 dB. To reduce the excess noise, we use an Erbium doped fiber amplifier. As previously mentioned, this amplifies the LO to the optimal working point of the homodyne detector (see Supplemental Material [29] for more details). The main contribution to the excess noise comes from residual phase noise due to the mismatch between the actual phase noise accumulated in the fiber and its estimation during our process of compensation (see Supplemental Material [29] for more details).

In our system, we adopt a high-precision phase compensation scheme in order to (i) eliminate the phase shift induced from the unbalanced MZI structure and (ii) decrease the phase noise as much as possible. In this way, we can achieve long-distance transmission where even a slight increase of the excess noise may have nontrivial degradation effects on the value of the secret key rate. To reduce this residual phase noise, we switch the key signals (i.e., those used for key generation) with higher-intensity 'reference signals' that are specifically dedicated to phase noise estimation. In our setup, the variance V_A of the Gaussian modulation of the key signals as well as the signal-to-noise ratio (SNR) of the reference signals are controlled by modulators AM$_1$ and AM$_4$, which are in turn controlled by a 10-bit digital-analog-converter (DAC). In our phase compensation scheme, a series of specific phase reference frames modulate the AM$_1$ to generate 100 reference pulses every 1000 data pulses. With the help of AM$_4$, the final SNR of the reference pulses is 34 dB higher than that of the signal pulses. Note, sending higher-intensity references pulses here will not increase more practical security problems

than sending weak-intensity references pulses [27]. With this value, the residual phase noise is low enough to support the system over 202.81 km fiber. The results of the homodyne detection are used for calculating the relative phase difference between transmitted and received data, and the phase modulator on the LO path at Bob's side modulates Bob's data according to the calculated phase estimation results.

Once Bob has measured the states sent from Alice, the two parties postprocess their data to generate a secret key [6]. In a CV-QKD system, postprocessing can be divided into four parts: basis sifting, parameter estimation, information reconciliation (or error correction), and privacy amplification. In our system, parameter estimation is performed after error correction (apart from a preliminary estimation of the SNR).

Results. − From the correlated data, we compute the covariance matrix illustrated in Fig. 2 from which we can derive the asymptotic key rate of our system. Then taking finite-size effects into account, the reverse-reconciliation secret key rate is given by the general formula [3, 36]

$$K_{finite} = f\left(1 - \alpha\right)\left(1 - FER\right)\left[\beta I\left(A:B\right) - \chi\left(B:E\right) - \Delta\left(n\right)\right],$$
(1)

where f is the repetition rate, α is the system overhead quantifying the ratio between reference and key signals, FER is the frame error rate of the reconciliation, β is the reconciliation efficiency, $I(A : B)$ is the classical mutual information between Alice and Bob, $\chi(B : E)$ bounds Eve's Holevo information on Bob's variable in the finite-size regime, and $\Delta(n)$ is an offset term which accounts for privacy amplification in the finite-size regime. Here we build corresponding maximum-likelihood estimators for the channel parameters, compute their confidence intervals, and bound their values adopting 6.5 standard deviations. This worst-case scenario is then used to evaluate Eve's Holevo bound.

Highly efficient postprocessing is needed to achieve long transmission distances at sufficiently high secret key rates. Polar codes and multi-edge type LDPC codes are used to obtain high reconciliation efficiencies at the intermediate distances (see Supplemental Material [29] for more details). For extremely low SNRs (lower than −26 dB), error correction is very difficult and it becomes challenging to construct suit-
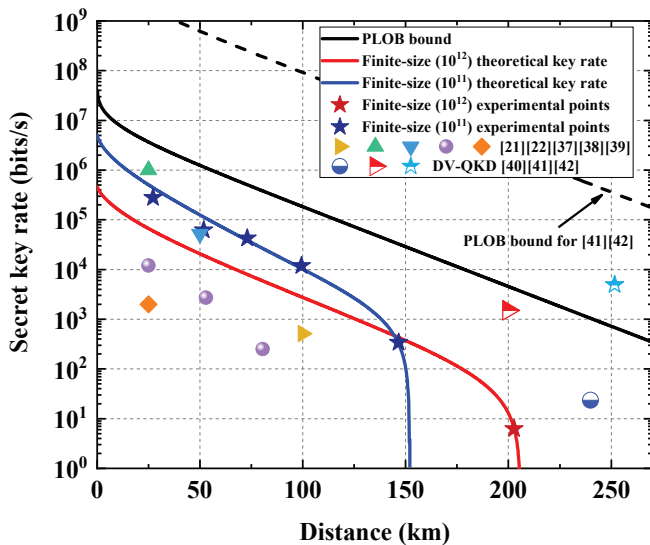
FIG. 3. Experimental key rates and numerical simulations. The six five-pointed stars correspond to the experimental results at different fiber lengths of 27.27 km, 49.30 km, 69.53 km, 99.31 km, 140.52 km, and 202.81 km. The blue solid curve is a numerical simulation of the key rate which is computed starting from the experimental parameters at 140.52 km. The red solid curve is the corresponding numerical simulation computed from the parameters at 202.81 km. For comparison, we also show previous state-of-the-art CV-QKD experimental results [21, 22, 37–39], DV-QKD experimental results from 200 km to 250 km [40–42], and we compare the values and the scaling of our rates with the PLOB bound [43], i.e., the fundamental limit of repeaterless quantum communications. In particular, the PLOB bound is plotted with respect to our clock rate (5 MHz, black solid line) and with respect to the clock rate of Ref. [41, 42] (2.5 GHz, black dashed line).

ably fixed-rate error correcting codes. For this reason, for our longest distance, we resort to a Raptor code. This is a type of rateless code able to reach high reconciliation efficiency by sending check information until error correction is successful. In order to extract secret key at low SNR (lower than -26 dB), we use the reconciliation scheme that combine multidimensional reconciliation and Raptor codes. Alice and Bob divide their data into vectors of size eight and normalized them. A binary random sequence c is generated by a quantum random number generator. The sequence c is then encoded into another sequence U through Raptor encoding. Bob uses U and his own Gaussian variable Y' to calculate the mapping function $M(Y', U)$. After Alice received enough side information, she starts to recover U by Raptor decoding and, therefore, Bob's random binary sequence c. The rate of Raptor codes is uncertain before information transmission. In this work, we set the expected reconciliation efficiency to 98% and the length of the encoded sequence is 1.82×10^6. We achieved high efficient reconciliation error correction with the optimal degree distribution of Raptor code. Then, in the step of privacy amplification, we use hash function (Toeplitz matrices in our scheme) to distill the final key at speed 1.35 Gbps using graphic processing unit after error correction.

The overview of experimental parameters and performance for different fiber lengths is shown in TABLE I. The secret key rate is 278 kbps at 27.27 km (4.36 dB losses), 62.00 kbps at 49.3 km (8.29 dB losses), 42.8 kbps at 69.53 km (11.68 dB losses), 11.8 kbps at 99.31 km (15.89 dB losses) and 318.85 bps at 140.52 km (23.46 dB losses). For the longest transmission distance of 202.81 km (32.45 dB losses) in our experiment, there is a SNR of 0.0023, the modulation variance V_A is 7.65 SNU, and the excess noise is 0.0081 SNU, where SNU represents shot-noise units. Bob's detector is assumed to be inaccessible to Eve and it is characterized by an electric noise of 0.1523 SNU and an efficiency of 0.6134. To obtain enough data, we run the system over seven periods corresponding to a total of 61.73 h of acquisition time (see Supplemental Material [29] for more details), including the necessary interruptions for alignment. This allowed us to extract 1380889 secret bits, which corresponds to a secret key rate of 6.214 bps.

The secret key rates of numerical simulations and experimental results are shown in Fig. 3. The five-pointed stars correspond to our experimental results at different fiber lengths. The blue ones are for 27.27 km and 49.3 km with a reconciliation efficiency of 95%, and for 69.53 km, 99.31 km, and 140.52 km with a reconciliation efficiency of 96%. The red one is instead for 202.81 km with 98% reconciliation efficiency. The blue and red solid curves are the numerical simulations calculated from experimental parameters at 140.52 km and 202.81 km with optimal postprocessing, respectively. We compare our points with the previous state-of-the-art CV-QKD experimental results [21, 22, 37–39], DV-QKD experimental results from 200 km to 250 km [40–42], and we also show their behaviour with respect to the PLOB bound [43], i.e., the secret key capacity of the bosonic lossy channel and fundamental limit of repeaterless quantum communications. Note that the current record of 502 km in optical fiber has been achieved by the phase-matching DV-QKD of Ref. [44], which is not a one-way protocol but exploits an intermediate twin field node [45].

Conclusion. − In conclusion, our long distance experiment has extended the security range of a CV-QKD system to the record fiber-distance of 202.81 km, a distance that closes the gap with the performance of current one-way QKD protocols with discrete variable systems. In addition, thanks to optimization procedures at the optical layer (phase compensation) and highly-efficient postprocessing techniques, the secret key rates are higher than previous results in CV-QKD at almost all distances. It is worth to remark that these key rates have been achieved with a repetition rate of only 5 MHz, therefore much slower than the clocks used in discrete-variable experiments (of the order of 1 GHz or more). While there are still several challenging techniques to achieve high-speed CV-QKD system, such as shot-noise-limited homodyne detector, high-speed postprocessing, and precise parameter estimation, our results pave the way for an implementation of CV-QKD in more practical settings and show that large-scale secure QKD networks are within reach of room-temperature standard telecom components.

[1] C. H. Bennett and G. Brassard, in Proc. IEEE Int. Conf. on Computers, Systems and Signal Processing 175−179 (IEEE Press, 1984).

[2] A. K. Ekert, Phys. Rev. Lett. **67**, 661−663 (1991).

[3] S. Pirandola, U. L. Andersen, L. Banchi, M. Berta, D. Bunandar, R. Colbeck, D. Englund, T. Gehring, C. Lupo, C. Ottaviani, J. Pereira, M. Razavi, J. S. Shaari, M. Tomamichel, V. C. Usenko, G. Vallone, P. Villoresi, and P. Wallden, Advances in Quantum Cryptography, arXiv:1906.01645 (2019).

[4] F. Xu, X. Ma, Q. Zhang, H.-K. Lo, and J.-W. Pan, arXiv preprint arXiv:1903.09051 (2019).

[5] G. Zhang, J. Y. Haw, H. Cai, F. Xu, S. M. Assad, J. F. Fitzsimons, X. Zhou, Y. Zhang, S. Yu, J. Wu, W. Ser, L. C. Kwek, and A. Q. Liu, Nature Photon. **13**, 839-842 (2019).

[6] Y. Zhang, Z. Li, Z. Chen, C. Weedbrook, Y. Zhao, X. Wang, Y. Huang, C. Xu, X. Zhang, Z. Wang, M. Li, X. Zhang, Z. Zheng, B. Chu, X. Gao, N. Meng, W. Cai, Z. Wang, G. Wang, S. Yu, and H. Guo, Quantum Sci. Technol. **4**, 035006 (2019).

[7] F. Karinou, H. H. Brunner, C.-H. F. Fung, L. C. Comandar, S. Bettelli, D. Hillerkuss, M. Kuschnerov, S. Mikroulis, D. Wang, C. Xie, M. Peev, and A. Poppe, IEEE Photonics Technology Letters **30**(7), 650−653 (2018).

[8] T. A. Eriksson, T. Hirano, B. J. Puttnam, G. Rademacher, R. S. Luís, M. Fujiwara, R. Namiki, Y. Awaji, M. Takeoka, N. Wada, and M. Sasaki, Communications Physics **2**(1), 9 (2019).

[9] C. Weedbrook, S. Pirandola, R. García-Patrón, N. J. Cerf, T. C. Ralph, J. H. Shapiro, and S. Lloyd, Rev. Mod. Phys. **84**, 621 (2012).

[10] P. K. Lam and T. C. Ralph, Nature Photon., **7**, 350−352 (2013).

[11] V. C. Usenko and R. Filip, Entropy **18**, 20 (2016).

[12] F. Grosshans and P. Grangier, Phys. Rev. Lett. **88**, 057902 (2002).

[13] F. Grosshans, G. Van Assche, and J. Wenger, *et al.*, Nature **421**, 238 (2003).

[14] C. Weedbrook, A. M. Lance, W. P. Bowen, T. Symul, T. C. Ralph, and P. K. Lam, Phys. Rev. Lett. **93**, 170504 (2004).

[15] R. García-Patrón and N. J. Cerf, Phys. Rev. Lett. **102**, 130501 (2009).

[16] S. Pirandola, S. Mancini, S. Lloyd, and S. L. Braunstein, Nature Phys., **4**, 726−730 (2008).

[17] M. Navascuès, F. Grosshans, and A. Acín, Phys. Rev. Lett. **97**, 190502 (2006).

[18] R. García-Patrón and N. J. Cerf, Phys. Rev. Lett. **97**, 190503 (2006).

[19] F. Furrer, T. Franz, M. Berta, A. Leverrier, V. B. Scholz, M. Tomamichel, and R. F. Werner, Phys. Rev. Lett. **109**, 100502 (2012).

[20] A. Leverrier, Phys. Rev. Lett. **114**, 070501 (2015).

[21] P. Jouguet, S. Kunz-Jacques, A. Leverrier, P. Grangier, and E. Diamanti Nature Photon., **7**, 378−381 (2013).

[22] D. Huang, P. Huang, D. Lin, and G. Zeng, Scientific Reports **6**, 19201 (2016).

[23] Y. Zhang, Y. Huang, Z. Chen, Z. Li, S. Yu, and H. Guo, Phys. Rev. Applied **13**, 024058 (2020).

[24] http://www.corning.com

[25] X. C. Ma, S. H. Sun, M. S. Jiang, and L. M. Liang, Phys. Rev. A **88**, 022339 (2013).

[26] P. Jouguet, S. Kunz-Jacques, and E. Diamanti, Phys. Rev. A **87**, 062313 (2013).

[27] B. Qi, P. Lougovski, R. Pooser, W. Grice, and M. Bobrek, Phys. Rev. X **5**, 041009 (2015).

[28] D. B. S. Soh, C. Brif, P. J. Coles, N. Lütkenhaus, R. M. Camacho, J. Urayama, and M. Sarovar, Phys. Rev. X **5**, 041010 (2015).

[29] See Supplemental Material at [url] for the details of shot-noise-limited high-gain homodyne detector, phase drifting and experimental excess noise results, high efficient information reconciliation at different distances, which include Ref. [27, 28, 30–35].

[30] C. Zhou, X. Wang, Y. Zhang, G. Zhang, S. Yu, H. Guo, Phys. Rev. Applied **12**, 054013 (2019).

[31] X. Wang, Y. Zhang, Z. Li, B. Xu, S. Yu, H. Guo, Quantum Inf. Comput. **17**, 1123 (2017).

[32] M. Milicevic, Phd Thesis, University of Toronto (2017).

[33] M. Milicevic, C. Feng, L. M. Zhang, and P. G. Gulak, npj Quantum Information **4**, 21 (2017).

[34] G. V. Assche, J. Cardinal, N. J. Cerf, IEEE Transactions on Information Theory 50(2), 394-400 (2004).

[35] A. Leverrier, R. Alléaume, J. Boutros, G. Zémor, P. Grangier, Phys. Rev. A 77(4), 042325 (2008).

[36] A. Leverrier, F. Grosshans, and P. Grangier, Phys. Rev. A **81**, 062343 (2010).

[37] C. Wang, D. Huang, P. Huang, D. Lin, J. Peng, and G. Zeng, Sci. Rep. **5**, 14607 (2015).

[38] D. Huang, D. Lin, C. Wang, W. Liu, S. Fang, J. Peng, P. Huang, and G. Zeng, Opt. Express **23**, 17511 (2015).

[39] J. Lodewyck, M. Bloch, R. García-Patrón, S. Fossier, E. Karpov, E. Diamanti, T. Debuisschert, N. J. Cerf, R. Tualle-Brouri, S. W. McLaughlin, and P. Grangier, Phys. Rev. A **76**, 042305 (2007).

[40] B. Fröhlich, M. Lucamarini, J. F. Dynes, L. C. Comandar, W. W.-S. Tam, A. Plews, A. W. Sharpe, Z. Yuan, and A. J. Shields, Optica **4**, 163−167 (2017).

[41] A. Boaron, B. Korzh, R. Houlmann, G. Boso, D. Rusca, S. Gray, M.-J. Li, D. Nolan, A. Martin, and H. Zbinden, Appl. Phys. Lett. **112**, 171108 (2018).

[42] A. Boaron, G. Boso, D. Rusca, C. Vulliez, C. Autebert, M. Caloz, M. Perrenoud, G. Gras, F. Bussières, M.-J. Li, D. Nolan, A. Martin, H. Zbinden, Phys. Rev. Lett. **121**, 190502 (2018).

[43] S. Pirandola, R. Laurenza, C. Ottaviani, and L. Banchi, Nature communications **8**, 15043 (2017).

[44] X.-T. Fang, P. Zeng, H. Liu, M. Zou, W. Wu, Y.-L. Tang, Y.-J. Sheng, Y. Xiang, W. Zhang, H. Li, Z. Wang, L. You, M.-J. Li, H. Chen, Y.-A. Chen, Q. Zhang, C.-Z. Peng, X. Ma, T.-Y. Chen, and J.-W. Pan, Nat. Photonics (2020). https://doi.org/10.1038/s41566-020-0599-8

[45] M. Lucamarini, Z. Yuan, J. F. Dynes, A. J. Shields, Nature **557**, 400−403 (2018).